Supporting Information

Pressure-Engineered Migration Bottlenecks and Non-Monotonic Ionic Conduction in NASICON Solid Electrolytes

Qiaoxin Zhang,[a] Huacai Yan,[*a] Mohan Jia,[a] Dequan Jiang,[a] Ke Liu,[b] Run Yu,[b] Yifeng An,[a] Tianyao Pei,[b] Yonggang Wang[*a]

[a] *State Key Laboratory of Advanced Waterproof Materials, School of Materials Science and Engineering, Peking University, Beijing 100871, China.*

[b] *Center for High Pressure Science and Technology Advanced Research (HPSTAR), Beijing 100193, China.*

[*]Email address: *yanhc@pku.edu.cn* (Huacai Yan);

ygw@pku.edu.cn (Yonggang Wang)

In situ HP EIS measurements

A symmetric diamond anvil cell (DAC) with 400 μm culets was employed for *in situ* HP EIS measurements. The sample chamber was prepared by pre-indenting a stainless steel gasket to 40 μm in thickness and laser-drilling a 250 μm diameter hole at its center. Insulating layers were fabricated by compacting epoxy-bonded cubic boron nitride (*c*-BN) powder into the gasket hole, followed by laser milling a sample chamber with 160 μm in diameter and 50 μm in thickness. A parallel-plate capacitor configuration with platinum (Pt) electrodes was used for measurements[1, 2]. Pressure was calibrated via ruby fluorescence. *In situ* HP EIS measurements were performed using a Metrohm Multi Autolab M204 electrochemical workstation, applying a 0.1 mV bias voltage across a frequency range of 10^{-1} to 10^{6} Hz.

In situ HP XRD and Raman spectra measurements

The same size DAC was utilized to measure the *in situ* HP XRD and Raman spectra. For both measurements, a stainless steel gasket was pressed to 40 μm thickness and drilled with a 250 μm diameter hole to serve as the sample chamber. Silicone oil served as the pressure transmitting medium (PTM) during the experiments. For the *in situ* HP XRD measurements, data were collected at room temperature by a focused monochromatic X-ray beam (0.6199 Å) at beamline station BL15U1 of the Shanghai Synchrotron Radiation Facility (SSRF). Pressure was calibrated via ruby fluorescence during compression. The data were collected using a MAR345 image plate detector, with CeO_2 as the calibration standard. The obtained two-dimensional XRD patterns were integrated using Dioptas software[3], and lattice parameters at different pressures were refined by Fullprof[4]. For the *in situ* Raman spectra, measurements were conducted at room temperature by a Renishaw inVia reflex mico-Raman spectroscope with 532 nm laser excitation, and the Raman signal of Si was used as the calibrated standard.

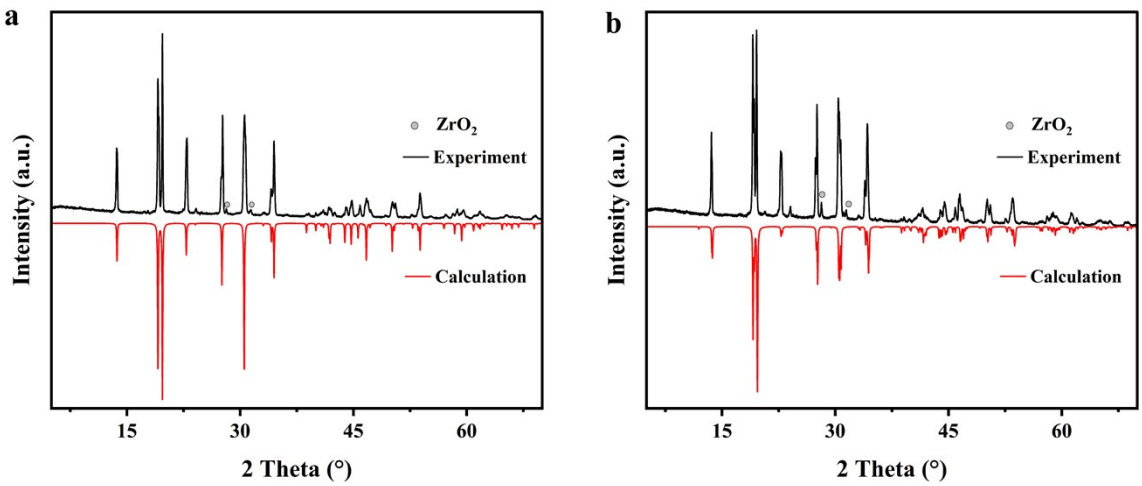

Fig. S1 Powder XRD pattern for (a) NZSP-*R*-3*c* and (b) NZSP-*C*2/*c*.

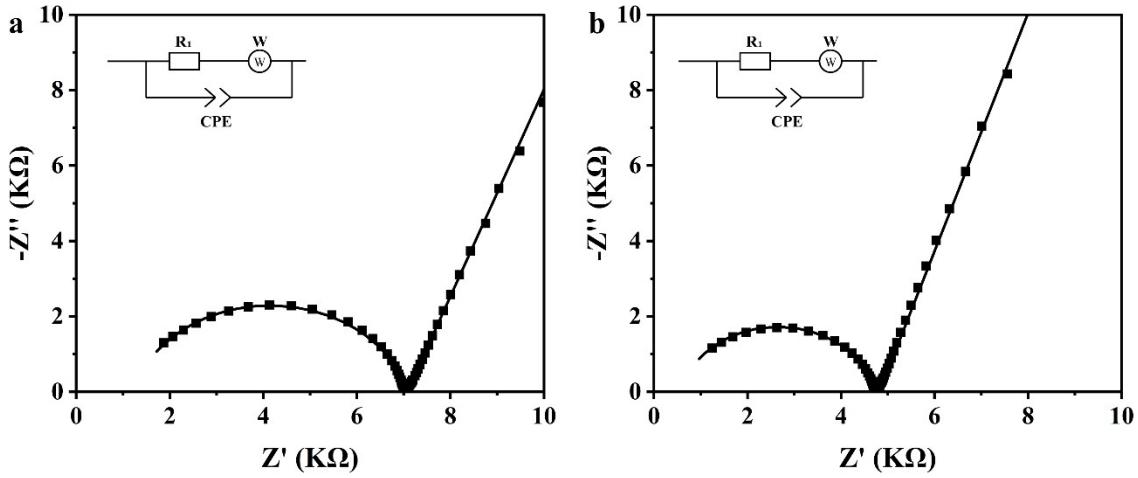

Fig. S2 EIS of the two ceramic pellets. Nyquist plots, fitting curves for (a) NZSP-*R*-3*c* and (b) NZSP-*C*2/*c* under ambient conditions. Inset: Equivalent circuit.

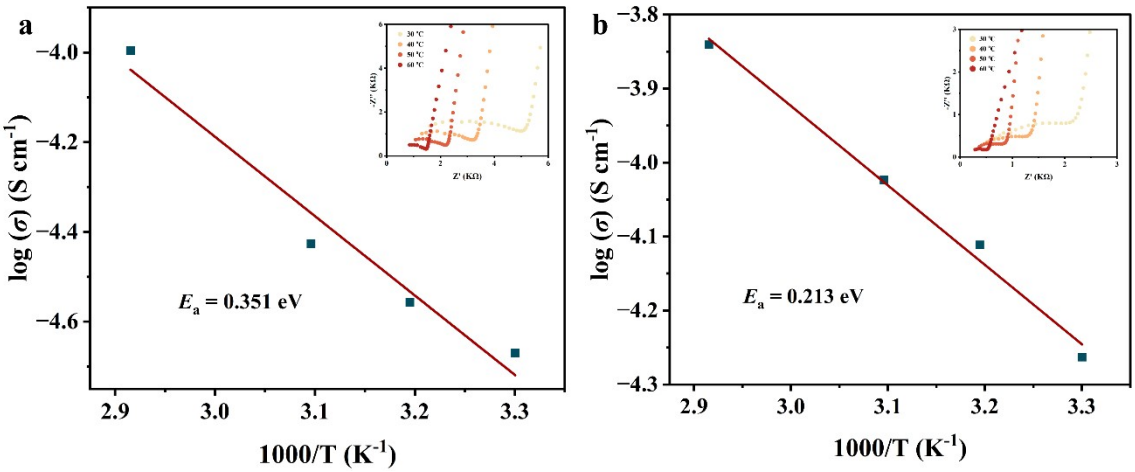

Fig. S3 Arrhenius plots of ionic conductivity for (a) NZSP-*R*-3*c* and (b) NZSP-*C*2/*c* from 30 °C-60 °C under ambient conditions. Insets: Nyquist plots from 30 °C-60 °C.

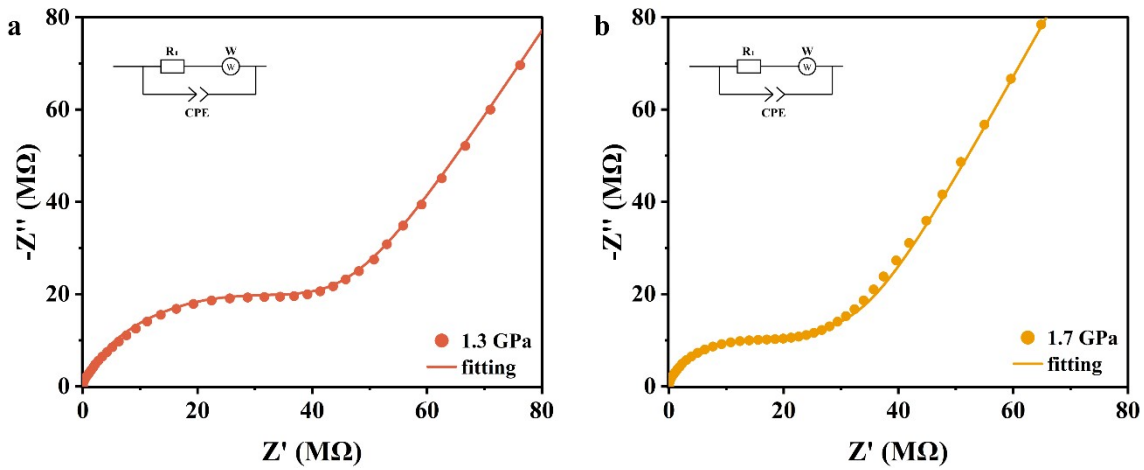

Fig. S4 Representative EIS with Nyquist plot analysis. Nyquist plots with fitting curves for (a) NZSP-*R*-3*c* at 1.3 GPa and (b) NZSP-*C*2/*c* at 1.7 GPa. Inset: Equivalent circuit.

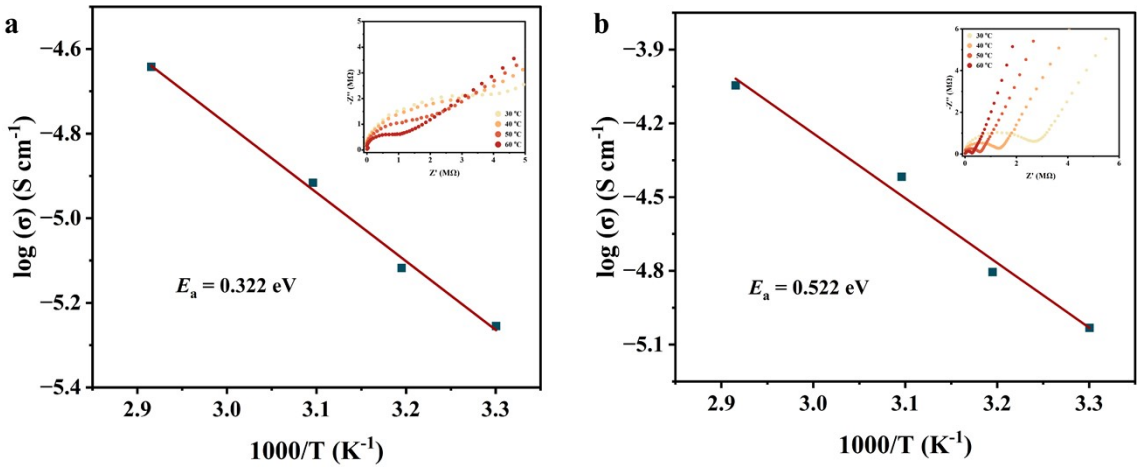

Fig. S5 Arrhenius plots of ionic conductivity for NZSP-*C*2/*c* from 30 °C-60 °C at (a) 0.2 GPa and (b) release to 0.4 GPa. Insets: Nyquist plots of NZSP-*C*2/*c* from 30 °C-60 °C.

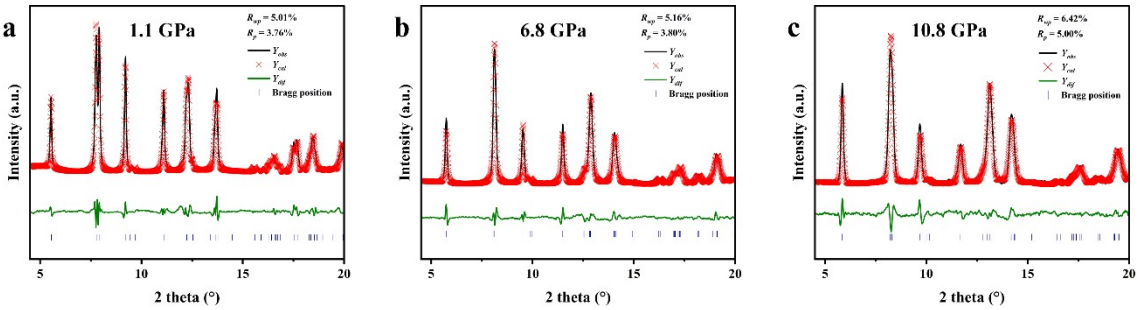

Fig. S6 LeBail fittings for the XRD patterns of NZSP-*R*-3*c* at selected pressures.

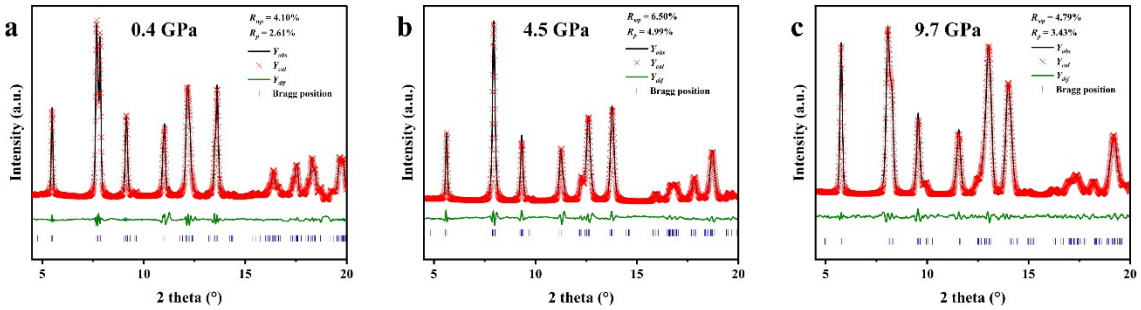

Fig. S7 LeBail fittings for the XRD patterns for NZSP-*C*2/*c* at selected pressures.

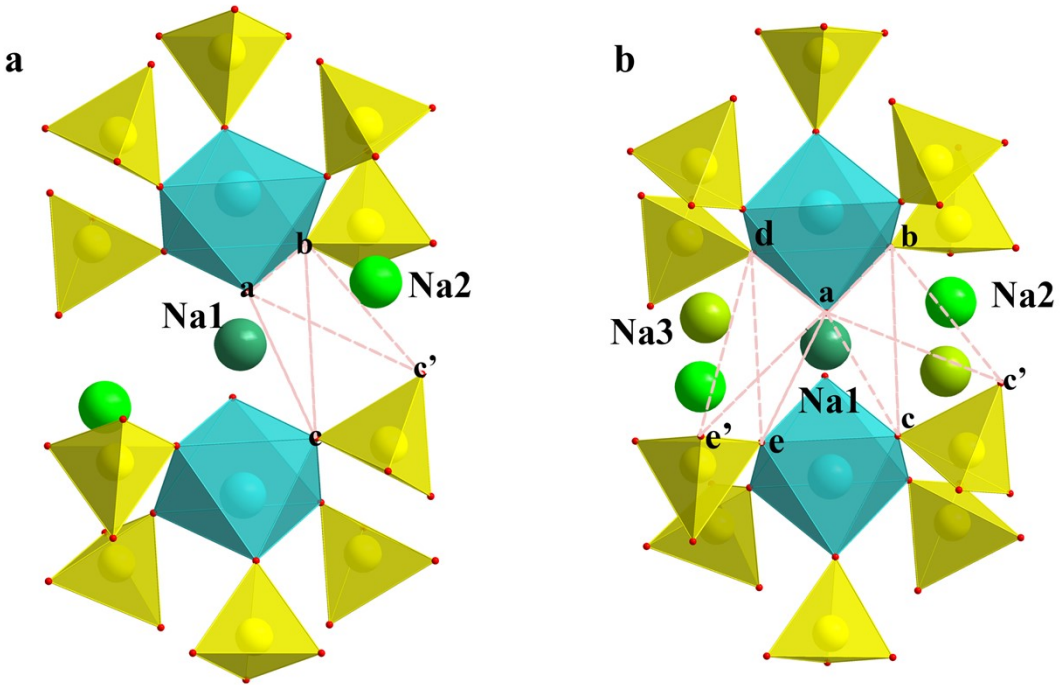

Fig. S8 Local structural geometries with bottlenecks extracted from (a) NZSP-*R*-3*c* and (b) NZSP-*C*2/*c*.

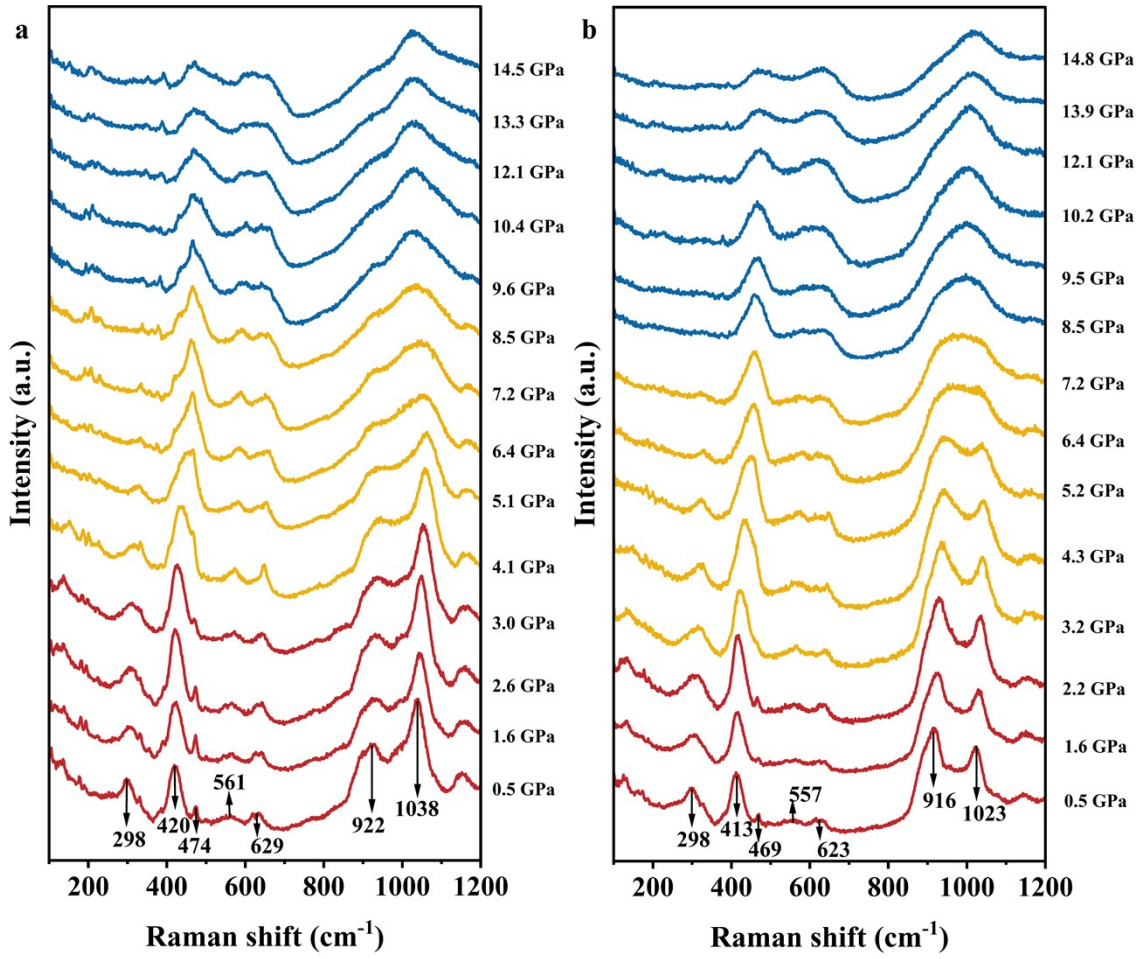

Fig. S9 *In situ* HP Raman spectra at room temperature for (a) NZSP-*R*-3*c* and (b) NZSP-*C*2/*c*.

Table S1. Pressure effects on bottleneck dimensions extracted from NZSP-*R*-3*c*.

	0 GPa	3 GPa	6 GPa		0 GPa	3 GPa	6 GPa
ab (Å) (Triangle A)	2.877	2.822	2.778	ab (Å) (Triangle B)	2.877	2.822	2.778
bc (Å) (Triangle A)	3.992	3.894	3.805	bc’ (Å) (Triangle B)	3.66	3.593	3.54
ac (Å) (Triangle A)	3.992	3.894	3.805	ac’ (Å) (Triangle B)	4.308	4.243	4.188
∠abc (°) (Triangle A)	68.878	68.753	68.59	∠abc’ (°) (Triangle B)	81.512	81.878	82.105
∠bac (°) (Triangle A)	68.878	68.753	68.59	∠bac’ (°) (Triangle B)	57.159	56.944	56.826
∠bca (°) (Triangle A)	42.243	42.493	42.821	∠bc’a (°) (Triangle B)	41.329	41.178	41.069
Area ($Å^2$) (Triangle A)	5.353	5.12	4.922	Area ($Å^2$) (Triangle B)	5.205	5.015	4.865

Table S2. Pressure effects on bottleneck dimensions extracted from NZSP-*C*2/*c*.

	0 GPa	3 GPa	6 GPa		0 GPa	3 GPa	6 GPa
ab (Å) (Triangle A)	2.874	2.820	2.776	ab (Å) (Triangle B)	2.874	2.820	2.776
bc (Å) (Triangle A)	4.018	3.901	3.8	bc’ (Å) (Triangle B)	3.712	3.638	3.578
ac (Å) (Triangle A)	4.021	3.902	3.801	ac’ (Å) (Triangle B)	4.343	4.272	4.212
∠abc (°) (Triangle A)	69.097	68.829	68.583	∠abc’ (°) (Triangle B)	81.446	81.762	81.979
∠bac (°) (Triangle A)	69.001	68.807	68.581	∠bac’ (°) (Triangle B)	57.680	57.446	57.281
∠bca (°) (Triangle A)	41.901	42.364	42.839	∠bc’a (°) (Triangle B)	40.874	40.792	40.74
Area (Å2) (Triangle A)	5.396	5.132	4.91	Area (Å2) (Triangle B)	5.277	5.075	4.917
ad (Å) (Triangle C)	2.872	2.820	2.776	ad (Å) (Triangle D)	2.872	2.820	2.776
de (Å) (Triangle C)	4.022	3.903	3.801	de’ (Å) (Triangle D)	3.715	3.64	3.579
ae (Å) (Triangle C)	4.018	3.901	3.80	ae’ (Å) (Triangle D)	4.342	4.272	4.212
∠dae (°) (Triangle C)	68.995	68.793	68.574	∠dae’ (°) (Triangle D)	81.377	81.737	81.971
∠ade (°) (Triangle C)	69.115	68.849	68.588	∠ade’ (°) (Triangle D)	57.785	57.48	57.291
∠dea (°) (Triangle C)	41.85	42.358	42.838	∠de’a (°) (Triangle D)	40.838	40.783	40.738
Area (Å2) (Triangle C)	5.392	5.132	4.911	Area (Å2) (Triangle D)	5.274	5.079	4.919

Table S3. Raman modes in NZSP-*R*-3*c* and NZSP-*C*2/*c*.

Raman shift in NZSP-*R*-3*c*	Raman shift in NZSP-*C*2/*c*.	Group[5]
1038	1023	P-O asymmetric stretch mode (υ3 (F2))
922	916	Si-O asymmetric stretch mode (υ3 (F2))
629	623	P-O asymmetric bending vibrations (υ4 (F2))
561	557	Si-O asymmetric bending vibrations (υ4 (F2))
474	469	P-O symmetric bending vibrations (υ2 (F2))
420	413	P-O symmetric bending vibration (υ2 (E))
298	298	Si-O symmetric bending vibration (υ2 (E))

1. Y. Wang, Y. Han, C. Gao, Y. Ma, C. Liu, G. Peng, B. Wu, B. Liu, T. Hu, X. Cui, W. Ren, Y. Li, N. Su, H. Liu and G. Zou, *Rev. Sci. Instrum*., 2010, **81**, 013904.
2. Q. Wang, C. Liu, Y. Han, C. Gao and Y. Ma, *Rev. Sci. Instrum*., 2016, **87**, 123904.
3. C. Prescher and V. B. Prakapenka, *High Pressure Res.*, 2015, **35**, 223-230.
4. J. Rodriguezcarvajal, *Phys. B*, 1993, **192**, 55-69.
5. K. Nakamoto, Infrared and Raman Spectra of Inorganic and Coordination Compounds, John Wiley & Sons, Ltd, 2006.